PostPrint. Jie Cheng, et al. Chemical Engineering Science, Volume 281 (2023) 119133
https://doi.org/10.1016/j.ces.2023.119133

Capturing CO_2 by Ionic Liquids and Deep Eutectic Solvents: A Comparative Study Based on Multi-level Absorbent Screening

Jie Cheng[a], Kunchi Xie[a], Pengyu Guo[a], Hao Qin[c], Liyuan Deng[d], Zhiwen Qi[a,*], Zhen Song[a,b,*]

[a]*State Key laboratory of Chemical Engineering, School of Chemical Engineering, East China University of Science and Technology, 130 Meilong Road, Shanghai 200237, China*

[b]*Engineering Research·Center of Resource Utilization of Carbon-containing Waste with·Carbon Neutrality (Ministry of Education), East China University of Science and Technology 130 Meilong Road, Shanghai 200237, China*

[c]*Process Systems Engineering, Otto-von-Guericke University Magdeburg, Universitätsplatz 2, D-39106 Magdeburg, Germany*

[d]*Department of Chemical Engineering, Norwegian University of Science and Technology, Sem Sælandsvei 4, 7491 Trondheim, Norway*

Corresponding authors: *zwqi@ecust.edu.cn; songz@ecust.edu.cn*

Abstract: Because of the high energy consumption and volatility of organic amine solvents in conventional CO_2 capture processes, ionic liquids (ILs) and deep eutectic solvents (DESs) have been widely expected as alternative CO_2 absorbents. In this work, promising ILs and DESs are identified through a comparative, multi-level absorbent screening method proposed for the first time from a large space of cation-anion combinations and potential DES components, respectively. Important physical properties (namely melting point, viscosity, and toxicity) of potential ILs and salt components of DESs are estimated by a recently-reported deep learning model. Key thermodynamic properties including physically-based absorption and desorption potentials as well as eutectic behaviors between DES component combinations are predicted by the COSMO-RS model. Five EHS (environment, health, and safety) related properties of non-salt components of DESs are assessed by the VEGA platform. From above, the top three ILs and DESs are identified from 5440 and 38389 candidates, respectively. The CO_2 capture processes based on the retained ILs and DESs are simulated in Aspen Plus in rate-based mode, identifying 1-methyl-1-propylpyrrolidinium bromide: methylimidazole (1:2) as the absorbent with the highest process performance. The experiments shows that the molality-based Henry constant of CO_2 in DES is as low as 1.32, validating the competitive absorption performance of this potential DES. Finally, quantum chemistry calculations are conducted to unveil the microscopic absorption mechanism.

Keywords: CO_2 capture; ionic liquid; deep eutectic solvent; multi-level absorbent screening; absorption experiments; IGM analysis

PostPrint. Jie Cheng, et al. Chemical Engineering Science, Volume 281 (2023) 119133
https://doi.org/10.1016/j.ces.2023.119133

Abbreviations

AC	absorption capacity
BCF	bioconcentration factor
CCS	carbon capture and storage
CCU	carbon capture and utilization
CNN	convolutional neural network
CO_2	carbon dioxide
COSMO-RS	Conductor-like Screening Model for Real Solvents
DE	desorption easiness
DESs	deep eutectic solvents
EHS	environment, health and safety
HBA	hydrogen bond acceptor
HBD	hydrogen bond donor
IGM	independent gradient model
ILs	ionic liquids
MEA	ethanolamine
N_2	nitrogen
SLE	solid-liquid phase equilibrium
SMILES	simplified molecular-input line-entry system
T_e	eutectic temperature
ΔH_{dis}	CO_2 dissolution enthalpy
η	viscosity
$[C_3MPYR][Br]$	1-methyl-1-propylpyrrolidinium bromide
$[(ETO)_2IM][Tf_2N]$	1,3-diethoxyimidazolium bis(trifluoromethylsulfonyl)imide
$[N_{1,1,1,1}][Cl]$	tetramethylammonium chloride
$[N_{1,1,3,2}$-OH$][Br]$	N-(2-hydroxyethyl)-N,N-dimethyl-N-propylammonium bromide

1. Introduction

Global warming has aroused widespread concerns around the world, which is mainly caused by the excessive emission of carbon dioxide (CO_2) (Dang et al., 2022; Kovačič et al., 2020). Currently, carbon capture, utilization and storge (CCUS) has been and is still considered as the most active method for reducing CO_2 emissions (Hu et al., 2021; Ješić et al., 2021; Liu et al., 2020a; Pavlišič et al., 2020; Psarras et al., 2017). In addition to direct air capture of CO_2 by adsorption methods (Sun et al., 2023), it is practically beneficial to reduce CO_2 emissions by absorption using organic amine solvents such as ethanolamine (MEA) for capturing CO_2 in flue gas (Dinda et al., 2010; Li et al., 2014; Singto et al., 2016; Zhao et al., 2023). However, such chemically-based absorption processes have several serious disadvantages including large solvent loss, high energy consumption for solvent regeneration, and corrosion of equipment (Cao et al., 2017; Chen et al., 2013; Han et al., 2013). Thus, from the green chemistry and sustainable development point of view, it is vital to seek alternative absorbents of organic amine solutions.

Ionic liquids (ILs) and deep eutectic solvents (DESs) have recently attracted significant attention for CO_2 capture (Ali et al., 2022; Castro et al., 2018; Huang et al., 2014) due to their flexible structure designability, low volatility, wide liquid temperature, etc. (Bezold and Minceva, 2018; Khan et al., 2023; Olugbemide et al., 2021; Song et al., 2019b; Ullah et al., 2017). Their properties can be tuned in a wide range either by changing cation-anion combinations or by mixing different potential components of hydrogen bond acceptors (HBA) and hydrogen bond donors (HBD) in different ratios (Paiva et al., 2014; Sarmad et al., 2017). These unique properties make them highly attractive options for many separation processes, including both chemically and physically based absorption of CO_2 (Taheri et al., 2018; Yu et al., 2020; Zhang et al., 2018). Although the chemical absorption of CO_2 based on ILs/DESs could overcome the drawbacks of organic amine solvents to some extent, the process for CO_2 desorption and solvent regeneration is still complicated by the underlying chemical reactions (Ban et al., 2014). In this sense, physical absorption of CO_2 by ILs and DESs has been widely studied concerning the advantages of simple equipment option and facile solvent regeneration (Pinto et al., 2014; Qin et al., 2021). For instance, Revelli et al. (2010) evaluated CO_2 solubility in four imidazolium-based ILs, among which $[(ETO)_2IM][Tf_2N]$ exhibits the highest CO_2 solubility (dissolving 122 g CO_2 in 1 kg ILs under the conditions of 313 K and 40 bar). Wang et al. (2019) studied the application of four phosphonium-based DESs as physical absorbents by experimentally measuring the solubility of CO_2 and molecular dynamics simulation, which proves that these DESs can absorb CO_2 effectively and their structures remain stable during the absorption process. However, as there are almost numerous potential ILs and DESs, experimental study of them one by one for CO_2 absorption is impossible.

For the purpose of quickly identifying promising ILs/DESs as physical

absorbents for CO_2, many researchers have reported related works recently (Qin et al., 2022; Song et al., 2019a; Wang et al., 2018; Yu et al., 2021). To give a few examples, Taheri et al. (2021) evaluated the selectivity of 5980 ILs for CO_2 and hydrogen sulfide based on the Henry constant calculation by COSMO-RS, and predicted the dissolution enthalpy of CO_2 in different ILs, from which the top two IL candidates were retained. Zhang et al. (2016) calculated the sensible heat and CO_2 working capacity based on the heat capacity and CO_2 solubility of ILs collected from literature, and seven out of 76 ILs were screened out with low energy consumption. Luo et al. (2021) obtained a promising DES for CO_2 absorption from 280 candidates by calculating the infinite dilution solubility using COSMO-RS, which was proved to be reliable from experimental vapor-liquid equilibria of DES-gas mixtures. Subsequently, the CO_2 absorption processes by the selected DES and MEA were compared in Aspen Plus, confirming that the DES is superior to MEA in terms of energy consumption and solvent recovery. Liu et al. (2020b) reviewed the experimental data on the solubility and Henry constant of CO_2 in ILs/DESs, based on which the COSMO-RS model was calibrated linearly to improve the prediction accuracy for screening CO_2 absorbents. Despite the progresses made, a comparative study on the application of ILs and DESs for CO_2 capture from a large-scale, multi-level absorbent screening is still lacking in literature to the best of our knowledge.

In consideration of the above aspects, this work specifically focuses on the comparison of screening ILs and DESs as physical absorbent for CO_2 capture, which mainly include the estimation of thermodynamic and physical properties, the process simulation and optimization, the experimental validation, and the microscopic mechanism exploration. A deep learning method reported very recently (Chen et al., 2023) is used to evaluate the physical properties of the involved ILs and salt components of DESs, including melting point (T_m), viscosity (η) and toxicity, while the VEGA platform is employed to evaluate the EHS (environment, health, and safety) impacts of the non-salt components of DESs. The Henry constant of CO_2 in ILs and DESs at different temperatures and the formation of eutectics between potential DES components are calculated by the COSMO-RS model. Based on the top-ranked ILs and DESs, process simulations for CO_2 capture are performed in Aspen Plus to identify the most promising absorbent. Experiments are carried out to validate the absorption performance and quantum chemical calculations are performed to unveil the microscopic mechanism of the screened absorbent for CO_2 capture.

2. Method

The research framework of this work is shown in Figure 1. First, a large set of cations and anions in the COSMObase and potential components of DESs reported in literature are exhaustively collected. Then, an integrated step is employed to screen ILs/DESs, which includes the calculation of thermodynamic properties (namely the absorption and desorption potentials, the CO_2 dissolution enthalpy, and the solid-liquid phase equilibria between potential DES components) via COSMO-RS, the

prediction of physical properties of ILs and salt components of DESs through a deep learning method, the evaluation of EHS-impacts of non-salt components by VEGA, and process simulations based on the top-ranked ILs/DESs are carried out in Aspen Plus. Finally, the screened absorbent undergoes the absorption experiment test and quantum chemical mechanism study. To better clarify the proposed method, more details involved in the framework are provided in the following.

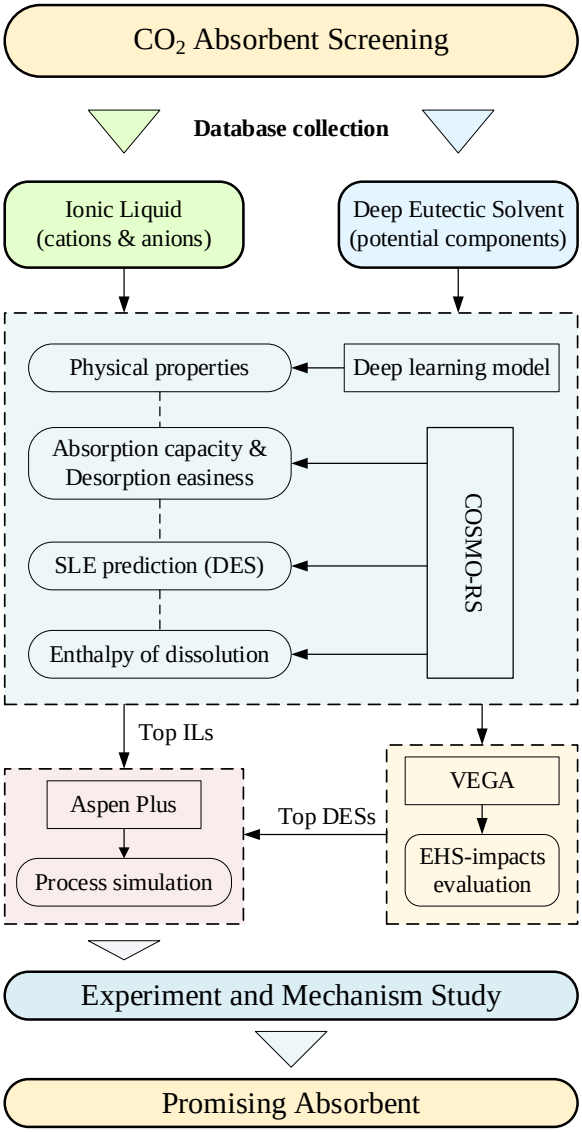

Figure 1. Research framework of this work.

2.1 Prediction of Thermodynamic Properties

Of central importance for selecting promising ILs/DESs as physical absorbent for CO_2 is to predict the thermodynamic properties of the IL/DES-involved systems. To this end, the COSMO-RS model is employed to predict the Henry constant of CO_2 in different ILs/DESs. As a statistical thermodynamics model based on the quantum chemical calculation, COSMO-RS is widely employed to predict the thermodynamic properties (e.g., infinite dilution activity coefficients, solubilities, and phase equilibria)

of fluid-liquid mixtures including IL/DES-involved systems (Diedenhofen and Klamt, 2010; Gerlach et al., 2018; Iqbal et al., 2019). Recent works have proved that COSMO-RS can qualitatively and semi-quantitively predict the Henry constant of CO_2 in ILs/DESs, satisfying the requirement for absorbent screening (Liu et al., 2020b; Liu et al., 2021; Taheri et al., 2021). Considering the introduction of COSMO-RS has already been described in detail in literature (Abranches et al., 2019; Klamt and Eckert, 2000; Klamt et al., 1998; Silva et al., 2018; Zhou et al., 2020), only the fundamentals of the thermodynamic properties calculated in this work are elaborated as follows.

For a given solute *i*, the Henry constant in the solvent *j* can be calculated as (Song et al., 2020b):

$$H_i^j = \frac{(\mu_i^{j,\infty} - \mu_i^{gas})}{RT} = \gamma_i^{j,\infty} p_i^0 \quad (1)$$

where $\mu_i^{j,\infty}$ and μ_i^{gas} are the chemical potentials of the solute *i* at infinite dilution in solvent *j* and ideal gas phase, $\gamma_i^{j,\infty}$ is the infinite dilution activity coefficient of solute *i* in solvent *j*, and p_i^0 is the vapor pressure of pure solute *i*. Based on the predicted Henry constant, two parameters namely absorption capacity (AC) and desorption easiness (DE) are employed as thermodynamic criteria for ILs/DESs screening:

$$AC = \frac{1}{H_{CO_2}^{298.15}} \times \frac{MW_{CO_2}}{MW_{candidate}} \quad (2)$$

$$DE = \frac{H_{CO_2}^{328.15}}{H_{CO_2}^{298.15}} \quad (3)$$

where $H_{CO_2}^{298.15}$ and $H_{CO_2}^{328.15}$ are the Henry constants of CO_2 in ILs/DESs at 298.15 K and 328.15 K; MW_{CO_2} and $MW_{candidate}$ represent the molecular weights of CO_2 and IL/DES candidates, respectively. Similar criteria have been demonstrated to be appropriate for screening ILs as absorbents (Jiang et al., 2021), and thus are directly adapted here. It should be noted that IL candidates are obtained by random combination of anions and cations, while DES candidates are constituted by the random combination of potential components in different molar ratios (e.g., 2:1, 1:1, 1:2 and 1:3 selected in this work).

To determine whether the potential component combinations can form room temperature liquid absorbent, the solid-liquid equilibrium (SLE) of each combination is predicted by COSMO-RS. Our recent work has proved that COSMO-RS is reasonable in the prediction of eutectic temperature (T_e) for systems involving different components, e.g., fatty/aromatic carboxylic acids, fatty alcohols, and pharmaceutical compounds (Song et al., 2021). This indicates that COSMO-RS could be used in this work to estimate whether the combinations of the potential components can form room-temperature DESs. Based on the SLE results, the component combinations that possess a T_e lower than 298.15 K and have a wide operating window are retained as potential room-temperature DESs.

Apart from the above-mentioned thermodynamic properties, the CO_2 dissolution

enthalpy (ΔH_{dis}) is also an important thermodynamic property related to the energy consumption in absorbent regeneration, which is composed of the CO_2 absorption enthalpy and excess enthalpy. Since the contribution of excess enthalpy to the ΔH_{dis} is usually less than 5% (Xie et al., 2014), the ΔH_{dis} can be simplified as (Oexmann and Kather, 2010; Zhang et al., 2016):

$$\Delta H_{dis} \approx \Delta H_{abs} = -RT^2\left(\frac{\partial lnH_{CO_2}(T)}{\partial(T)}\right) \quad (4)$$

where R is the gas constant and ΔH_{abs} represents the CO_2 absorption enthalpy. Moreover, $H_{CO_2}(T)$ and ΔH_{dis} can also be simplified as a quadratic function of the Henry constant with respect to temperature (Yan and Chen, 2010):

$$lnH_{CO_2}(T) = aT^{-2} + bT^{-1} + c \quad (5)$$

$$\Delta H_{dis} = -R\left(\frac{2a/T+b}{p_0}\right) \quad (6)$$

where a, b, and c are parameters of $lnH_{CO_2}(T)$, and p_0 is standard pressure. To regress the values of a, b and c, the Henry constant of CO_2 in ILs/DESs between 298.15 K and 328.15 K is further predicted by COSMO-RS with a step of every 5 K.

All the COSMO-RS calculations involved in this work are performed by the COSMOthermX (Version 19.0) at the BP86/TZVP level with the parameterization of BP_TZVP_C30_1901.ctd. The COSMO files of CO_2, anions/cations in ILs, and non-salt DES components are directly taken from the COSMObase (Version. 19.0, COSMOlogic GmbH), and those for the salt DES components are obtained by the Gaussian 09 software package (Version D.01) in the same manner as already introduced earlier (Song et al., 2021).

2.2 Assessment of Physical Properties and EHS-Impacts

The assessment of physical properties (e.g., melting point, viscosity, and toxicity) of ILs/DESs is also important to ensure that the retained IL/DES candidates are in liquid state, not too viscous at room temperature, and of potential sustainability. Different from many conventional molecules, the physical properties of most ILs/DESs are generally unknown (Chen et al., 2022; Ghanem et al., 2018; Khan et al., 2017; Wang et al., 2020b). In this work, an advanced deep learning method reported very recently (Chen et al., 2023) is used to predict the melting point, viscosity, and toxicity of ILs/salt components of DESs. To be specific, the deep learning method is a two-stage architecture of Transformer and convolutional neural network (CNN) (Chen et al., 2021) , wherein the Transformer is pretrained on a huge unlabeled database of the SMILES (simplified molecular-input line-entry system) of 9,434,070 IL-like molecules for capturing IL molecular fingerprints while the CNN is trained on labeled databases of IL properties. By case studies on eleven IL properties (including the three properties considered here), it was demonstrated that the Transformer-CNN method presents superior performance to state-of-the-art models and enables the quick prediction of IL properties. The mean absolute error between the predicted and experimental data for the considered properties in ten-fold cross validations are 11.15

K for melting point, 0.35 for viscosity (lnη in mPa·s), and 0.1126 for toxicity (in leukemia rat cell line evaluated by the logarithm of the half maximal effective concentration $\log_{10}EC_{50}$), respectively, which are all notably lower compared to reference models in literature. Note that, the only required input in the Transformer-CNN method is the SMILES of ILs (and temperature and/or pressure if needed). More details about the Transformer-CNN method for IL property prediction can be referred to Chen et al. (2023).

For non-salt DES components, the VEGA platform is employed to evaluate five EHS-related properties namely persistence, bioconcentration factor (BCF), mutagenicity, carcinogenicity, and toxicity. As a platform integrating dozens of quantitative structure-activity relationship (QSAR) models (Benfenati et al., 2019), VEGA only requires the SMILES as input information (Linke et al., 2020). Besides the quantitative or qualitative results for each property, the reliability of the results by each prediction model (e.g., experimental, good, moderate, and low) can also be provided by VEGA. For each of the five properties, the prediction results and reliability of different models implemented in VEGA are jointly evaluated, which can be divided into five grades (Song et al., 2020b). In short, the first three grades (i.e., green, blue, and purple) mean that the negative result of a property is of experimental/good reliability or is provided consistently by all available models; by contrast, the last two grades (i.e., yellow and red) mean that the positive result of a property is of experimental/good reliability or is provided consistently by all available models. To select non-salt DES components with potential EHS-compatibility, only the components with all five properties in the first three grades are selected, which are further checked in the PubChem database to eliminate other EHS-related concerns.

In this section, only the ILs meeting the melting point, viscosity and toxicity requirements (i.e., T_m < 298.15 K, η < 100 mPa·s and $\log_{10}EC_{50}$ > 3.4) are retained. As for DESs, only the combinations of salt components meeting the toxicity requirements and potentially EHS-compatible non-salt components can be retained.

2.3 Process Simulation for CO_2 Capture Based on ILs/DESs

For comparing the process performances of the screened ILs/DESs for CO_2 absorption, the continuous absorption processes based on ILs/DESs are established in Aspen Plus with a simplified dehydrated flue gas including CO_2 and nitrogen (N_2) as the feed gas (Luo et al., 2021; Ma et al., 2017). In this step, COSMO-SAC is selected as the thermodynamic method. The process simulation is performed in Aspen Plus V12 and the RadFrac with the rate-based mode is adopted as the absorber. The Koch Flexipac 700Y corrugated sheet structured packing is employed and the number of equilibrium stage is fixed as 10 (Higgins and Liu, 2015; Wang et al., 2020a). The flue gas components (CO_2 and N_2) are directly taken from the Aspen Plus database; ILs are defined as pseudo-components; DESs are considered as a mixture of salt and non-salt components, wherein the salt components are defined in the same way as ILs. The required physical parameters (namely boiling point, density, viscosity and critical

properties) of ILs/salt components of DESs are determined through the group contribution method developed by Valderrama et al (Valderrama and Robles, 2007; Valderrama et al., 2008). As methylimidazole (one non-salt component involved in the top-ranked DESs) is missing in Aspen Plus, its physical parameters are also estimated by COSMO-RS. The σ-profiles (SGPRF1 to SGPRF5) and the COSMO molecular volume (CSACVL) of all components are directly gained from the COSMObase. The optimal operating parameters of each process are determined by sensitivity analysis and design specifications.

2.4 Experiment of CO_2 Absorption

To validate the practical performance of the screened absorbent, the CO_2 absorption experiments are employed. The following is a brief introduction of the involved chemicals and the experimental procedure.

Methylimidazole (≥99%) is purchased from Macklin, [C_3MPYR][Br] (≥99%) is supplied by Adamas-beta, and the CO_2 cylinder (≥99.999%) is obtained from Shanghai Wetry Standard Reference Gas. The [C_3MPYR][Br] is treated by vacuum drying at 80 ℃ for 24 h to remove traces of volatile impurities and to ensure a low water content (<1000 ppm, as determined by Karl–Fischer titration) before use. Methylimidazole and CO_2 gas are used as received without further purification.

The screened DES is obtained by mixing [C_3MPYR][Br] and methylimidazole in a vial at a molar ratio of 1:2 (weighed by the Sartorius BSA224S-CW balance, ±0.0001 g), and stirring for 3 hours at 55 ℃ and 800 rpm until a clear and transparent liquid mixture is formed. The liquid mixture is then cooled to 25 ℃ to check whether it can maintain a homogeneous liquid phase. A pressure drop method is applied to determine the CO_2 solubility in DES (from 100 kPa to 1400 kPa) at 25 ℃ and 55 ℃ by employing the device illustrated in Figure S1 (Supporting Information). Initially, CO_2 from the cylinder is introduced into the gas reservoir with a sufficient time for temperature equilibration. Subsequently, the valve connecting the gas reservoir and the absorption tank is opened, and the experiment proceeds until the pressure reaches complete stabilization. Given the negligible vapor pressure of DES, the gas phase is treated as pure CO_2 and the CO_2 solubility in DES is calculated as:

$$n_{CO_2} = \left[\rho_{CO_2}(p_1,T)V_G - \rho_{CO_2}(p_2,T)(V_A + V_G - m_{DES}/\rho_{DES})\right]/m_{DES} \quad (7)$$

where n_{CO_2} is the CO_2 solubility in DES (g CO_2/g DES); $\rho_{CO_2}(p_1,T)$ and $\rho_{CO_2}(p_2,T)$ are the density of CO_2; V_A and V_G represent the volume of the gas reservoir and absorption tank; m_{DES} and ρ_{DES} denote the weight and the density of DES, respectively.

2.5 Quantum Chemical Calculations

After the previous screening steps, quantum chemical calculations can be performed to offer deep insight into the absorption mechanisms of the screened absorbent. The geometric configurations at the lowest energy state of each individual component as well as the complexes of [C_3MPYR][Br], methylimidazole and CO_2 are obtained by the optimization using Gaussian 09 software package with the DFT-D3

dispersion corrections (Li et al., 2021; Song et al., 2020a; Zhang et al., 2019). All the geometries are preoptimized at B3LYP/6-31+G (d, p) theoretical level, and then the fully optimizations are carried out at B3LYP/6-311+G (d, p) theoretical level (Fu et al., 2021). The most stable structures of [C_3MPYR][Br], methylimidazole, {[C_3MPYR][Br] + methylimidazole + methylimidazole}, {[C_3MPYR][Br] + CO_2}, {methylimidazole + CO_2}, and {[C_3MPYR][Br] + methylimidazole + methylimidazole + CO_2} are identified by comparing different combination modes of geometric structures. Then, the interaction strength between DES and CO_2 is estimated by intermolecular interaction energy ($\Delta E_{binding}$), which is calculated as (Li et al., 2021):

$$\Delta E_{binding} = E_{DES+CO_2} - \left(E_{DES} + E_{CO_2}\right) + E_{BSSE} \quad (8)$$

where E_{DES+CO_2}, E_{DES}, E_{CO_2} and E_{BSSE} represent the energies of DES-CO_2 complex, pure DES, pure CO_2, and the basis set superposition error, respectively. Moreover, the independent gradient model (IGM) based on electron density analysis is adopted to analyze the noncovalent interactions between DES and CO_2 via the Multiwfn 3.8 program (Lu and Chen, 2012), intuitively reflecting the position and type of interactions.

3. Results and Discussion

3.1 IL Screening

From the COSMObase, 420 cations and 108 anions are collected to form IL candidates and summarized in Table S1 (Supporting Information). However, some of these ions are not widely seen in experimentally reported ILs. To screen ILs that are potentially purchasable or could be readily prepared, all ions are checked in Google Scholar, with the number of items that can be found as an empirical estimation of potential availability. As shown in Figure S2 (Supporting Information), most of these ions are located at the bottom (especially cations), which indicates that they have been scarcely reported and may be difficult to be prepared. In this context, the number of items found larger than 100 is empirically taken as a criterion for a prescreening of the ions. Correspondingly, 64 cations and 85 anions from the initial ions database are retained.

By randomly combining the prescreened cations and anions, 5440 IL candidates can be obtained. To evaluate their potential as CO_2 absorbent, the melting point, viscosity and toxicity of all the IL candidates are predicted by the Transformer-CNN model, while their AC and DE are calculated by the COSMO-RS model. The detailed prediction results for these properties are summarized in Table S2 (Supporting Information). Figure 2 illustrates the predicted results on AC, DE, viscosity, and melting point of all the involved IL candidates. As seen, the properties of the IL candidates vary in a large range and generally show inconsistent trends from case to case (that is, many ILs cannot satisfy all desirable properties). This finding highlights the importance of searching promising ILs from a large database of potential candidates. In the screening here, the melting point and viscosity are set to be lower

than the absorption temperature (298.15 K) and 100 mPa·s at 298.15 K, while the toxicity in terms of $\log_{10}EC_{50}$ is set to be higher than 3.4, respectively. Considering these constraints, 94 of the 5440 IL candidates are retained.

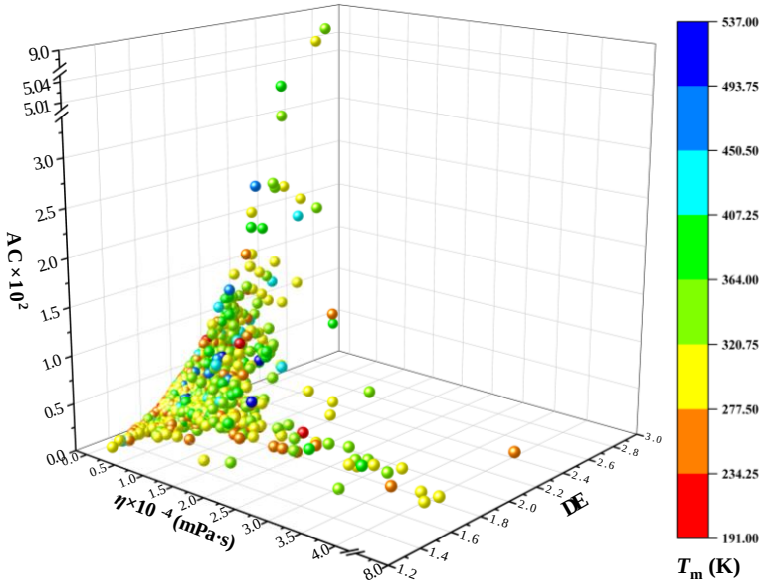

Figure 2. Predicted absorption capacity (AC), desorption easiness (DE), melting points (T_m) and viscosity (η) of 5440 ILs.

For further screening of ILs, AC, DE and ΔH_{dis} are comprehensively considered to evaluate the absorption and desorption capacities of different ILs for CO_2 (see Table S3, Supporting Information). As illustrated in Figure 3, most of the ILs are located in the lower left corner, which indicates that these ILs possess inferior absorption and desorption potentials for CO_2. In this step, the upper bound of ΔH_{dis} is set to 15 kJ/mol to ensure the retained IL candidates generally require low energy consumption in the regeneration step. To get ILs with high absorption and desorption potentials, the searching direction is from the upper right corner to the lower left corner with ΔH_{dis} lower than 15 kJ/mol as a constraint. Table 1 summarizes the top three IL candidates (see chemical structures in Figure S3, Supporting Information), which will be subsequently evaluated by process simulation in Aspen Plus.

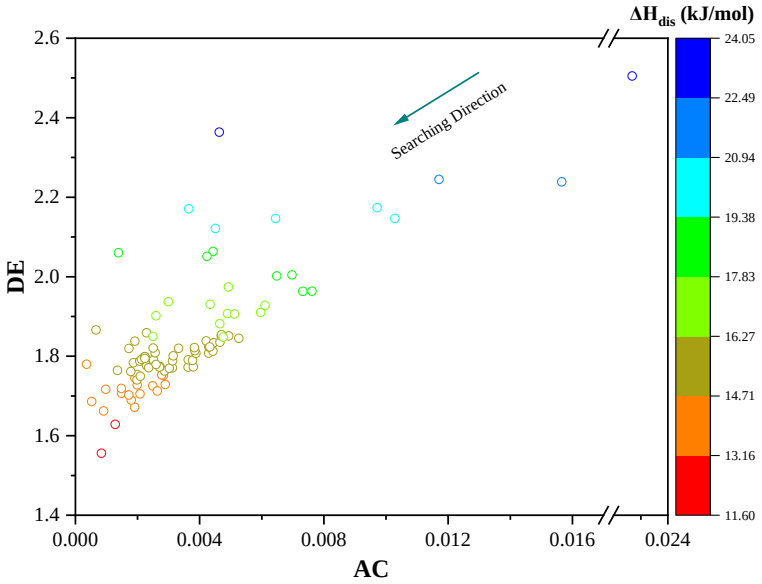

Figure 3. Predicted absorption capacity (AC), desorption easiness (DE), and CO_2 dissolution enthalpy (ΔH_{dis}) of 94 ILs.

Table 1. Top three IL candidates retained after screening of physical and thermodynamic properties.

	Cation	Anion	AC	DE	ΔH_{dis} (kJ/mol)
IL1	1-butyl-pyridinium	tricyanomethane	0.0038	1.7733	14.9973
IL2	1-propylpyridinium	tricyanomethane	0.0036	1.7724	14.9558
IL3	1-butyl-imidazolium	tricyanomethane	0.0031	1.7706	14.8749

3.2 DES Screening

After a detailed review of the literature (Abranches et al., 2020; Aroso et al., 2016; Klamt et al., 1998; Luo et al., 2021; Wang et al., 2019; Zhang et al., 2018; Zhou et al., 2020), 78 salt components and 120 non-salt components (detailed in Table S4, Supporting Information) are collected as the initial database of DES components, based on which various potential DESs can be formed by random combination of these components in different molar ratios. In addition to the typical combination of salt and non-salt components, thymol and menthol (Abranches et al., 2020; Aroso et al., 2016) were also reported to be able to form DESs combining with non-salt components. Therefore, all salt components as well as thymol and menthol are considered to combine with other non-salt components at the molar ratios of 2:1, 1:1, 1:2, and 1:3, leading to 38389 potential DES candidates (detailed in Table S5, Supporting Information). The AC and DE calculated by COSMO-RS are shown in Figure 4, where only the DES candidates with both AC and DE ranking top 10% are retained (marked in red circles) in this step. The corresponding lower bounds for AC

and DE are 0.0033 and 1.81, respectively. Accordingly, 1823 of the 38389 DES candidates are kept, involving 34 salt and 98 non-salt components.

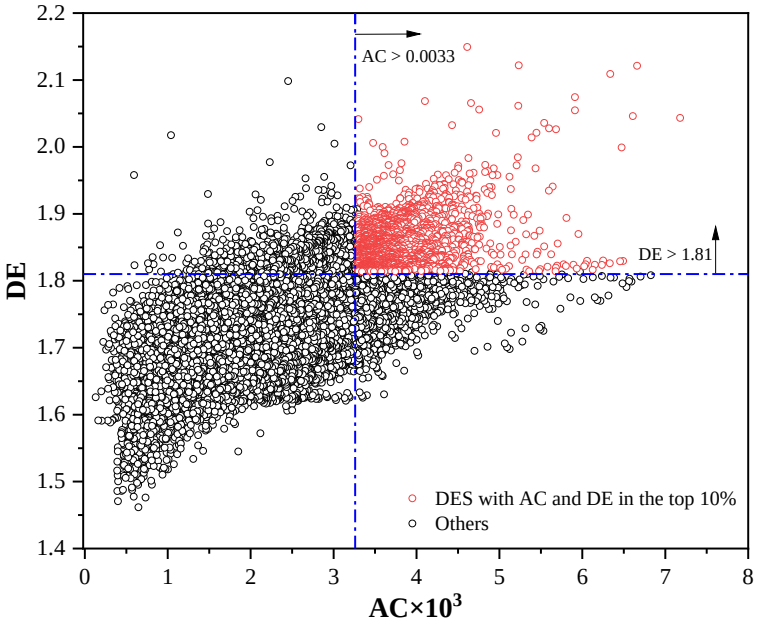

Figure 4. Predicted absorption capacity (AC) and desorption easiness (DE) of 38389 DES candidates.

The EHS impacts of 98 non-salt components involved in the above retained DES candidates are evaluated by use of the VEGA platform. The detailed calculation result and grade table of the five EHS-related properties are summarized in Table S6 and S7 (Supporting Information), respectively. By the constraints that all the five EHS-related properties should be in the first three grades (green, purple and blue), 39 of the 98 non-salt components survive for further evaluation. After reviewing them in the PubChem database, 12 of them are eliminated due to other potential hazards like flammability, health hazards, etc. The retained 27 non-salt components are involved in 490 of the 1823 DES candidates that rank top 10% in both AC and DE. These 490 DES candidates involve 29 salt components, for which the toxicity is estimated by the Transformer-CNN model (detailed in Table S4, Supporting Information). Similar to ILs, salt components of DESs with $\log_{10}EC_{50}$ below 3.4 are discarded. As a result, 239 of the 490 DES candidates are kept after this step.

To check whether the selected DES candidates can be applied as absorbent at 298.15 K, it is necessary to estimate melting point of them. For this purpose, SLE calculations are performed by COSMO-RS. The 239 DES candidates retained above involve 105 combinations of salt and non-salt components. The binary SLE of these combinations are calculated to obtain the eutectic point and the potential operating window at 298.15 K (detailed in Table S8). As the eutectic temperature is the lowest temperature that a binary combination can reach, only the combinations with eutectic temperature lower than 298.15 K are considered as potential room-temperature DESs. It should be noted that the eutectic points of some combinations are not predictable by COSMO-RS as the minimum temperature of SLE calculation in COSMOthermX is

set to be 100 K by default. However, such cases could generally indicate a very low eutectic temperature of the related binary combinations, and thus could also be considered applicable under room temperature. As a result, 190 out of the 239 DES candidates survive.

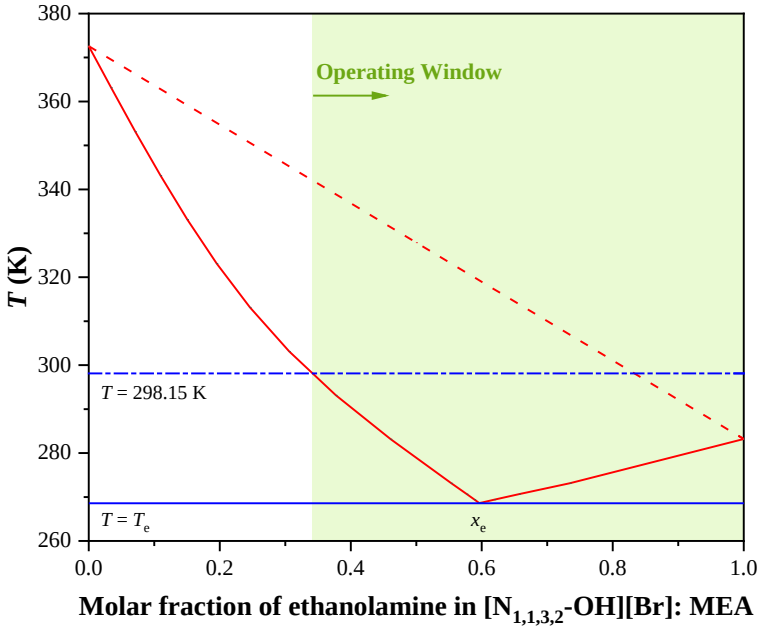

Figure 5. Solid-liquid phase equilibria of [$N_{1,1,3,2}$-OH][Br]: MEA predicted by COSMO-RS.

In addition to the eutectic temperature, the operating window, that is, the range of molar compositions that the binary combination can remain as liquid under room temperature is also an important factor in choose DES candidates. Figure 5 presents the SLE of the [$N_{1,1,3,2}$-OH][Br]: MEA combination as an example. As seen, with x_{MEA} from 0.34 to 1, the liquidus curves of the binary combinations are all in the region of T< 298.15 K, indicating an operating window of 0.66 of x_{MEA} compositions (as shaded in light green) for this system. The larger the operating window, the more likely the involved DES candidates could fall within the liquid phase region under room temperature. Empirically, an operating window higher than 0.3 is set as a criterion for desirable combinations of DES components. Correspondingly, 26 of the 105 salt and non-salt component combinations satisfy this criterion, retaining 49 of the 190 DES candidates.

To rank the top ones among the 49 DES candidates, the AC, DE and ΔH_{dis} of them are compared (see Figure 6 and Table S9). As the ΔH_{dis} for the 49 DES candidates are all higher than 15 kJ/mol, a relaxed constraint of 16.5 kJ/mol is taken. The searching direction is similar to that in the case of ILs screening, that is, from the upper right corner to the origin. Table 2 summarizes the AC, DE and ΔH_{dis} of the top three DES candidates (see chemical structures in Figure S4, Supporting Information), which will be evaluated subsequently by process simulation in Aspen Plus.

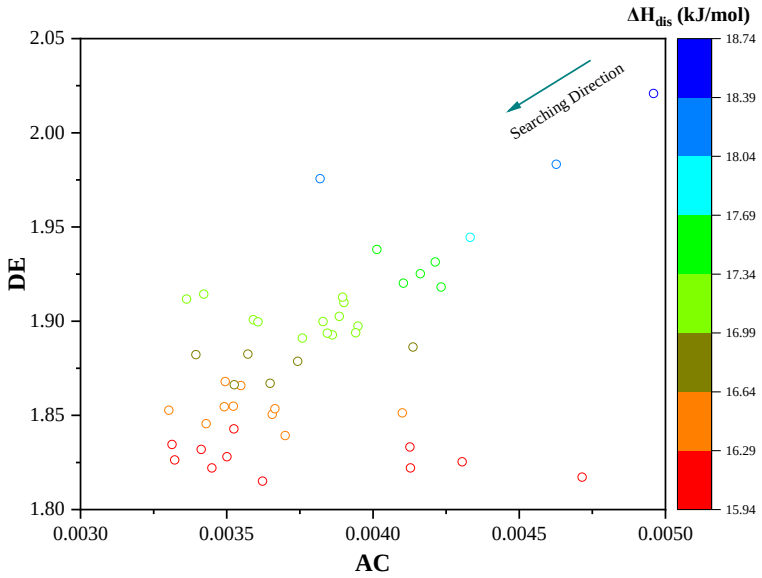

Figure 6. Predicted absorption capacity (AC), desorption easiness (DE), and CO_2 dissolution enthalpy (ΔH_{dis}) of 49 DESs.

Table 2. Top three DES candidates retained after screening of thermodynamic properties and EHS-impacts.

	HBA	HBD	Ratio	AC	DE	ΔH_{dis} (kJ/mol)
DES1	[$N_{1,1,3,2}$-OH][Br]	MEA	1:3	0.0047	1.8172	15.9965
DES2	[C_3MPYR][Br]	methylimidazole	1:2	0.0041	1.8513	16.4185
DES3	[$N_{1,1,3,2}$-OH][Br]	MEA	1:2	0.0043	1.8253	16.1148

3.3 Process Simulation Based on ILs or DESs

The process performances of the top-ranked IL and DES candidates in Tables 1 and 2 for CO_2 capture are further evaluated in Aspen Plus. In the simulated process, the dried flue gas is used as the feed gas, which is composed of CO_2 and N_2 with the molar fraction of 0.157: 0.843. The required physical properties of ILs and DESs, as predicted by the methods introduced in Section 2.3, can be found in Table S10 (Supporting Information). The amount of feed gas is 1000 kg/h. The design specifications are that the absorption ratio of CO_2 in the absorber is higher than 0.9, and the product purity of CO_2 and N_2 is higher than 0.9 and 0.95, respectively.

The CO_2 capture process based on IL/DES absorbent is shown in Figure 7. The feed gas enters the absorber from the bottom and contacts the IL/DES in countercurrent. The purified N_2 is obtained from the top of the absorber. The IL/DES after absorbing CO_2 flows into the flash1 to release the entrained N_2 and a small amount of CO_2, which return to the absorber. Subsequently, the CO_2-enriched IL/DES is transferred to flash2 to regenerate the IL/DES and obtain pure CO_2. The

regenerated IL/DES returns to the absorber after passing through the pump and the heat exchanger. It should be mentioned that the flash3 is an optional unit in the process. The MEA in DES1 and DES3 present a little volatility in the flash2, which requires the flash3 to release the MEA from the CO_2-enriched stream at 298.15 K and 1 bar. To keep consistent with the previous calculation of AC and DE by COSMO-RS, the absorption temperature in the absorber and the desorption temperature in the flash2 are set as 298.15 K and 328.15 K, respectively.

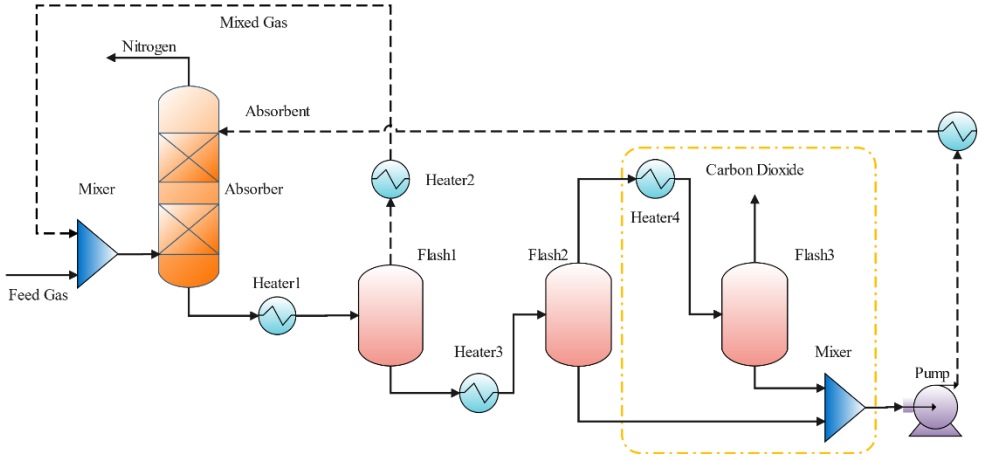

Figure 7. Flowsheet of CO_2 capture process based on IL/DES absorbent.

In the absorption process, the operating pressure, the column height, and mass ratio of absorbent to feed gas (L/G) all affect the absorption performance. Figure 8 presents the optimization of the absorber based on IL1. As seen, the blue lines represent the change of the absorption rate of CO_2 in the absorber with different column heights under the operating pressure of 5 bar and 20 bar, respectively. It can be seen that the CO_2 absorption rate increases with growing column height, and the rising rate is more palpable under high pressure. Nevertheless, if the column is high enough, a further height increase will only marginally increase the absorption rate. For instance, when the column height increases from 18 m to 19 m, the variation of the CO_2 absorption rate is less than 0.1% (even at the operating pressure of 20 bar). Considering the equipment cost of the absorber, the column height is fixed at 18 m to better compare the effects of different absorbents.

The red line in Figure 8 shows the dependency of L/G on the operating pressure under the design specifications (fixing the column height as 18 m). Obviously, a higher operating pressure is more favorable to reduce the required L/G, which on the flip side will also lead to the increase of operating cost. The operating pressure is empirically selected under such condition that the decrease of L/G is less than 1 for every 1 bar increase in operating pressure. Consequently, the operating parameters of the absorber are finally determined to be L/G=17.39 and 20 bar, respectively.

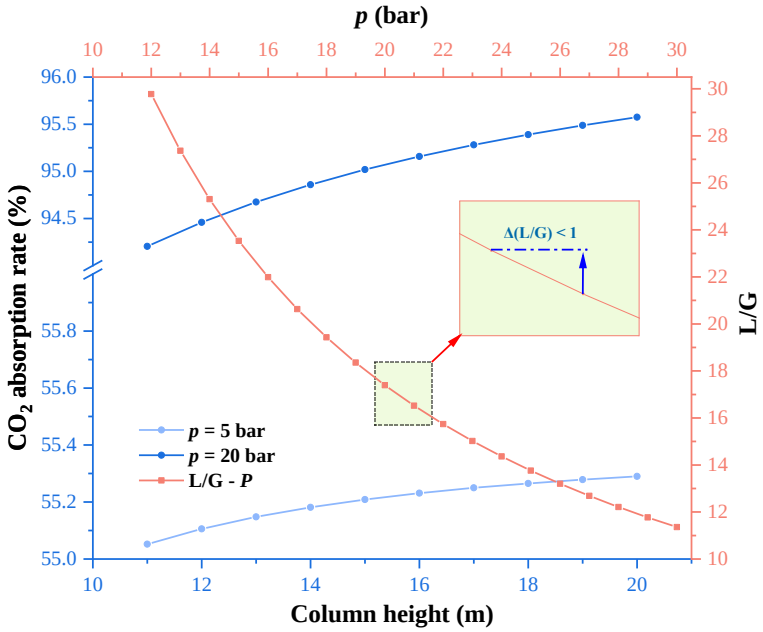

Figure 8. Effect of the operating pressure (red) and the column height (blue) in the absorber on the absorption ratio of CO_2.

To determine the operating temperature and pressure of the flash1, the mass flow of desorbed CO_2 (D_{CO2}) and N_2 (D_{N2}) at different conditions are calculated in Aspen Plus. Figure 9 shows the sensitivity analysis result of the flash1 of IL1-based process. As seen, the CO_2 purity of the bottom stream flowing out of the flash1 increases with the D_{N2}. Nevertheless, the desorption of N_2 is unfavorably accompanied with the increase in D_{CO2}, which will lead to the decrease in the CO_2 mass flow of the bottom stream. To maximize the mass flow of CO_2 entering the flash2, the D_{CO2} is limited to the minimum while ensuring the final CO_2 purity higher than 0.9. As a result, the operating temperature and pressure of the flash1 in IL1-based process are selected as 298.15 K and 12.2 bar.

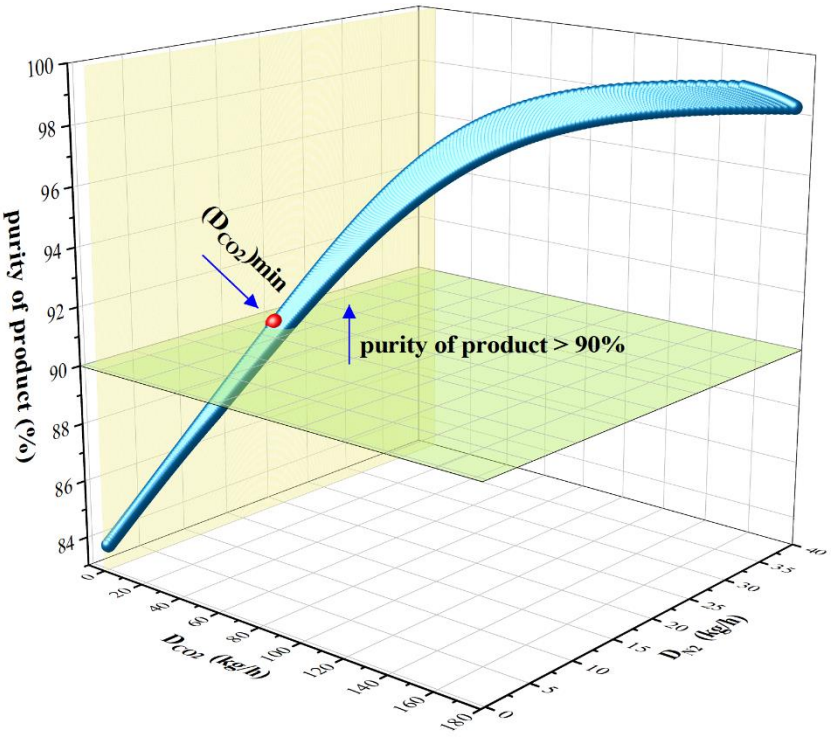

Figure 9. Effect of mass flow of CO_2 (D_{CO2}) and N_2 (D_{N2}) desorbed in the flash1 on the purity of the final CO_2 product in the IL1-based process.

The flash2 is employed to regenerate the ILs/DESs and obtain the CO_2 product. To get more CO_2 product, the purity of the regenerated ILs/DESs should be as high as possible. Figure S5 (Supporting Information) shows the effect of operating pressure on the purity of the regenerated IL1 with the desorption temperature at 328.15 K, which proves that the IL purity gradually increases with decreasing operating pressure. To ensure that CO_2 can be released as much as possible from the IL phase, the purity of the regenerated IL1 and the operating pressure are selected as 99.99 % and 0.05 bar, respectively.

Table 3 summarizes the optimized operating conditions and energy consumptions of the six CO_2 capture processes based on each of the top-ranked ILs/DESs. Compared with the thermal energy consumption in the process, the energy required for pumping is relatively much less. It is also noted that the required L/G of the absorber in DESs-based processes are lower than that in ILs-based processes and follows the sequence of IL1 < IL2 < IL3 and DES1 < DES3 < DES2. This is consistent with the result of the AC of the ILs/DESs, which indicates the reliability of the screening criteria. For the ILs-based processes, both the thermal and pumping energy consumption are distinctly higher than the DESs-based processes, which can be ascribed to the higher L/G of the absorber unit. Besides, the pressures of flash2 in the DESs-based processes are higher than the ILs-based processes due to the nonnegligible volatility of HBD components under low pressure, which will lead to the CO_2 recovery rates slightly lower than the ILs-based processes. Overall, the processes based on DES1 and DES2 rank the first in the required L/G and the energy

consumption, respectively. Considering that the equipment cost will increase with the requirement of the flash3 unit in DES1-based process, the DES2-based process could be considered as the most promising among the six studied processes. To wrap up, DES2 is finally identified as the most promising CO_2 absorbent among all the considered ILs/DESs in this work.

Table 3. Process simulation results of the CO_2 capture processes based on IL1 to IL3 and DES1 to DES3.

ILs/DESs	IL1	IL2	IL3	DES1	DES2	DES3
Absorption pressure/bar	20	20	23	15	17	15
L/G	17.39	17.86	19.96	13.02	14.34	13.25
Absorption temperature/K	298.15	298.15	298.15	298.15	298.15	298.15
Flash1 pressure/bar	12.2	13.1	12.3	10.7	11.5	11.2
Flash1 temperature/K	298.15	298.15	298.15	298.15	299.15	298.15
Flash2 pressure/bar	0.05	0.05	0.07	0.02	0.03	0.03
Flash2 temperature/K	328.15	328.15	328.15	328.15	328.15	328.15
Flash3 pressure/bar	-	-	-	1	-	1
Flash3 temperature/K	-	-	-	298.15	-	298.15
thermal energy/kW	248.78	254.29	275.45	220.48	162.85	196.71
pumping energy/kW	18.73	19.10	23.28	11.01	13.29	10.98

3.4 Experimental Verification and IGM Analysis

To further investigate the application potential of the screened DES2 for CO_2 absorption, a pressure drop method is employed to determine its solubility for CO_2 at 298.15 K and 328.15 K over a pressure range of 100 - 1400 kPa. As seen in Figure 10, the increase in pressure and the decrease in temperature are conducive to the absorption of CO_2 by DES2. Besides, the solubility of CO_2 in DES2 at 298.15 K is notably higher than that at 328.15 K. In other words, this CO_2 solubility difference shows that CO_2 can be desorbed from DES2 by simple heating.

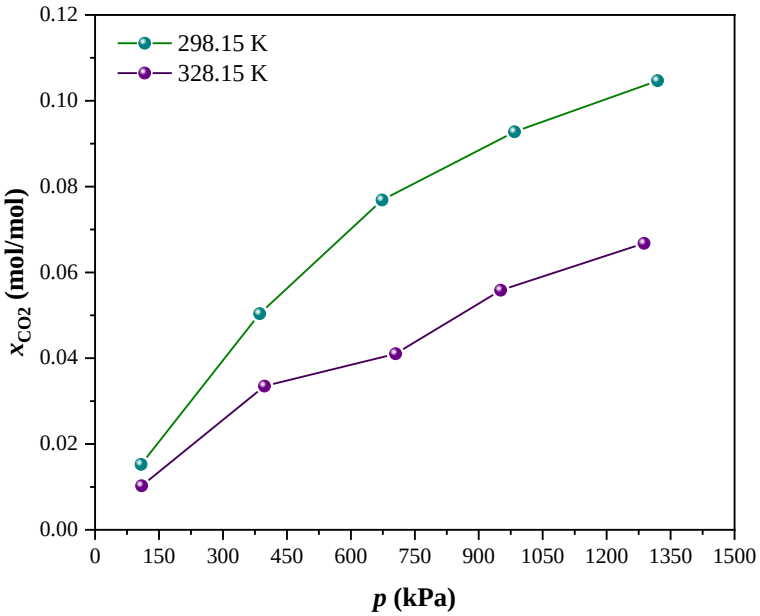

Figure 10. Solubility of CO_2 in the screened DES2.

Moreover, the molality-based Henry constant of CO_2 in DES2 at 298.15 K is calculated based on the measured solubility, and a comparison of DES2 with some DESs previously reported as physical absorbents in literature is made in Figure 11 (the detailed information of the involved DESs is listed in Table S11, Supporting Information). It is worth noting that some experimental data at 293.15 K and 303.15 K are supplemented for the limited data available at 298.15 K. As seen, the Henry constant of CO_2 in DES2 is lower than those in many DESs (even including some DESs at 293.15 K), indicating that DES2 has a satisfactory CO_2 absorption capacity. Although a few of the DESs exhibit a higher absorption capacity (i.e., a lower Henry constant of CO_2), DES2 has its potential advantages considering it is identified through rigorous screening criteria (including toxicity and EHS-impacts). To sum up, the DES2 could be regarded as a promising CO_2 absorbent.

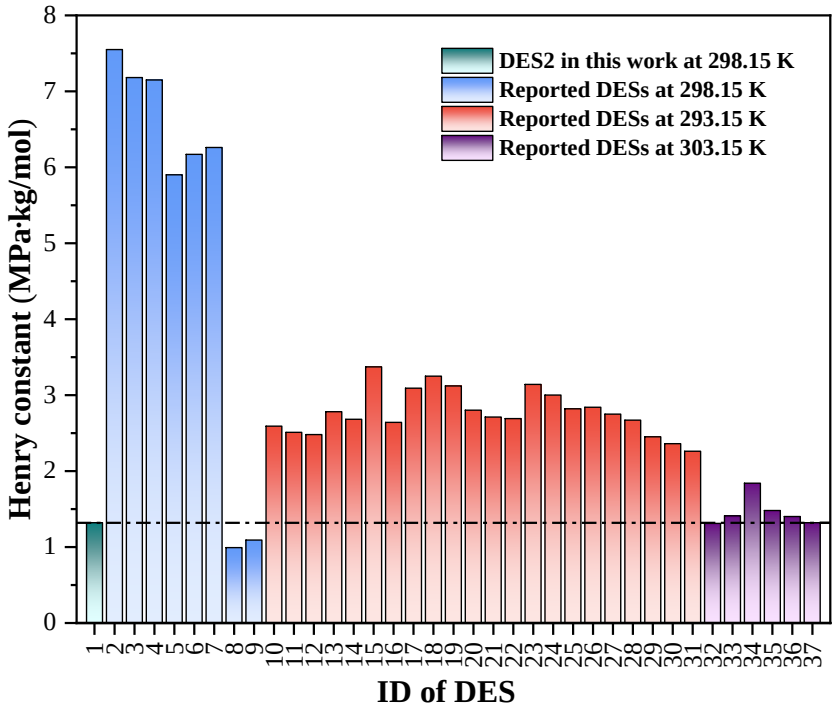

Figure 11. Comparison of the Henry constant in the DES2 at around 298.15 K with that in reported DESs.

To visually investigate the type and intensity of interactions between DES2 and CO_2, the color IGM diagram is generated via Multiwfn 3.8 program. As seen in Figure 12a, the hydrogen bond interactions (blue-green thick isosurfaces) in DES2 are mainly concentrated around the Cl atom. Additionally, some green thin isosurfaces are distributed between the [C_3MPYR][Br] and methylimidazole, indicating the presence of van der Waals interactions. Figure 12b, 12c and 12d display the interactions between [C_3MPYR][Br]/methylimidazole/DES2 and CO_2, respectively. It can be observed that van der Waals interactions are dominant while hydrogen bond interactions are relatively weak, which is consistent with the strong non-polarity of CO_2. The hydrogen bond and van der Waals interactions within DES2 are stronger than those between DES2 and CO_2, which indicates that CO_2 can be easily desorbed from DES2 without damaging the structure of DES2. Such IGM results well unravel the microscopic insights in the adsorption behaviors of CO_2 in DES2.

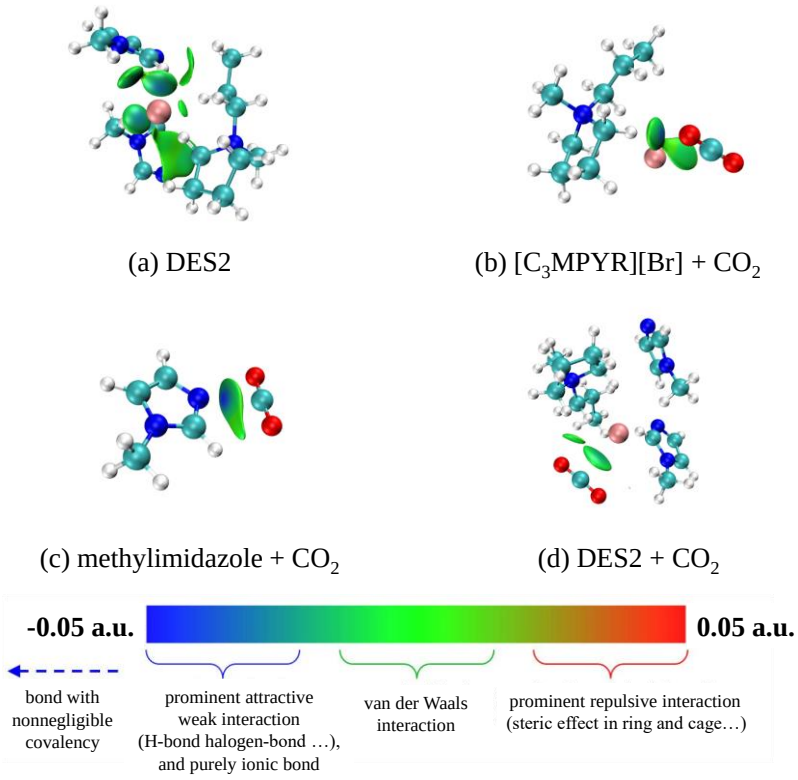

Figure 12. IGM analysis between DES2 and CO_2.

4. Conclusion

A comparative, multi-level absorbent screening study is for the first time presented to identify promising absorbents for CO_2 capture from a large pool of potential ILs and DESs. Among the 420 cations and 108 anions from the COSMObase, 64 cations and 85 anions are pre-screened based on potential availability, giving 5440 IL candidates. From the collection of experimentally reported DESs in literature, 78 salt components (together with thymol and menthol) and 120 non-salt components are selected to form 38389 potential DES candidates at four different molar ratios. By evaluating the melting point, viscosity and toxicity by the Transformer-CNN method, the EHS-impacts by VEGA, the absorption and desorption potentials, etc. by COSMO-RS, the top three IL and DES candidates are identified, respectively. After the process simulation of CO_2 capture based on these top-ranked absorbents, the DES2 [C_3MPYR][Br]: methylimidazole (1:2) with the lowest energy consumption and the second lowest solvent requirement is demonstrated as the most promising CO_2 absorbent. Finally, the high CO_2 absorption capacity of DES2 is validated by experiments, with a molar capacity of 0.11 and a molality-based Henry constant as low as 1.32 for CO_2 in DES2. At the same time, the nature of van der Waals interactions in the DES2-CO_2 system are unraveled by IGM analyses.

Considering the large space of the objectively obtained IL/DES candidates involved in the comparative screening, the results in this work basically suggest that

DESs could be considered as superior option to ILs for the physical absorption of CO_2. This present work could be a valuable reference for guiding the comparative selection of ILs and DESs for developing sustainable and energy efficient separation processes.

Supporting Information

Supporting Information to this article can be found online at ******.

Acknowledgements

This research is supported by the National Natural Science Foundation of China (NSFC) under the grants of 22208098, 21CAA01709, and 22278134.

References

Abranches, D.O., Larriba, M., Silva, L.P., Melle-Franco, M., Palomar, J.F., Pinho, S.P., Coutinho, J.A.P., 2019. Using COSMO-RS to design choline chloride pharmaceutical eutectic solvents. Fluid Phase Equilib. 497, 71-78. http://doi.org/10.1016/j.fluid.2019.06.005

Abranches, D.O., Martins, R.O., Silva, L.P., Martins, M.A.R., Pinho, S.P., Coutinho, J.A.P., 2020. Liquefying compounds by forming deep eutectic solvents: A case study for organic acids and alcohols. J. Phys. Chem. B 124, 4174-4184. http://doi.org/10.1021/acs.jpcb.0c02386

Ali, S.A., Mulk, W.U., Ullah, Z., Khan, H., Zahid, A., Shah, M.U.H., Shah, S.N., 2022. Recent advances in the synthesis, application and economic feasibility of ionic liquids and deep eutectic solvents for CO_2 capture: A review. Energies 15. http://doi.org/10.3390/en15239098

Aroso, I.M., Silva, J.C., Mano, F., Ferreira, A.S., Dionisio, M., Sa-Nogueira, I., Barreiros, S., Reis, R.L., Paiva, A., Duarte, A.R., 2016. Dissolution enhancement of active pharmaceutical ingredients by therapeutic deep eutectic systems. Eur. J. Pharm. Biopharm. 98, 57-66. http://doi.org/10.1016/j.ejpb.2015.11.002

Ban, Z.H., Keong, L.K., Mohd Shariff, A., 2014. Physical Absorption of CO_2 capture: A review. Advanced Materials Research. 917, 134-143. http://doi.org/10.4028/www.scientific.net/AMR.917.134

Benfenati, E., Roncaglioni, A., Lombardo, A., Manganaro, A., 2019. Integrating QSAR, read-across, and screening tools: The VEGAHUB platform as an example, in: Hong, H. (Ed.), advances in computational toxicology. Springer International Publishing, Cham, pp. 365-381.

Bezold, F., Minceva, M., 2018. Liquid-liquid equilibria of n-heptane, methanol and deep eutectic solvents composed of carboxylic acid and monocyclic terpenes. Fluid Phase Equilib. 477, 98-106. http://doi.org/10.1016/j.fluid.2018.08.020

Cao, L.D., Gao, J.B., Zeng, S.J., Dong, H.F., Gao, H.S., Zhang, X.P., Huang, J.H., 2017. Feasible ionic liquid-amine hybrid solvents for carbon dioxide capture. Int. J. Greenh. Gas Con. 66, 120-128. http://doi.org/10.1016/j.ijggc.2017.09.015

Castro, V.I.B., Mano, F., Reis, R.L., Paiva, A., Duarte, A.R.C., 2018. Synthesis and physical and thermodynamic properties of lactic acid and malic acid-based natural deep eutectic solvents. J. Chem. Eng. Data 63, 2548-2556. http://doi.org/10.1021/acs.jced.7b01037

Chen, G., Song, Z., Qi, Z., Sundmacher, K., 2023. Generalizing property prediction of ionic liquids from limited labeled data: a one-stop framework empowered by transfer learning. Digital Discovery. http://doi.org/10.1039/d3dd00040k

Chen, G.Z., Song, Z., Qi, Z.W., 2021. Transformer-convolutional neural network for surface charge density profile prediction: Enabling high-throughput solvent screening with COSMO-SAC. Chem. Eng. Sci. 246, 117002. http://doi.org/10.1016/j.ces.2021.117002

Chen, J.H., Zhu, F.Y., Qin, H., Song, Z., Qi, Z.W., Sundmacher, K., 2022. Rational eutectic solvent design by linking regular solution theory with QSAR modelling. Chem. Eng. Sci. 262. http://doi.org/10.1016/j.ces.2022.118042

Chen, Z.H., Deng, S.B., Wei, H.R., Wang, B., Huang, J., Yu, G., 2013. Activated carbons and amine-modified materials for carbon dioxide capture - A review. Front. Env. Sci. Eng. 7, 326-340. http://doi.org/10.1007/s11783-013-0510-7

Dang, Y.X., Tan, P., Hu, B., Gu, C., Liu, X.Q., Sun, L.B., 2022. Low-energy-consumption temperature swing system for CO_2 capture by combining passive radiative cooling and solar heating. Green Energy Environ. http://doi.org/10.1016/j.gee.2022.08.004

Diedenhofen, M., Klamt, A., 2010. COSMO-RS as a tool for property prediction of IL mixtures-A review. Fluid Phase Equilib. 294, 31-38. http://doi.org/10.1016/j.fluid.2010.02.002

Dinda, S., Goud, V.V., Patwardhan, A.V., Pradhan, N.C., 2010. Kinetics of reactive absorption of carbon dioxide with solutions of 1,6-hexamethylenediamine in polar protic solvents. Sep. Purif. Technol. 75, 1-7. http://doi.org/10.1016/j.seppur.2010.07.002

Fu, H., Hou, Y.P., Sang, H.N., Mu, T.C., Lin, X.F., Peng, Z.H., Li, P., Liu, J.H., 2021. Carbon dioxide capture by new DBU-based DES: The relationship between ionicity and absorptive capacity. AIChE J. 67. http://doi.org/10.1002/aic.17244

Gerlach, T., Muller, S., Smirnova, I., 2018. Development of a COSMO-RS based model for the calculation of phase equilibria in electrolyte systems. AIChE J. 64, 272-285. http://doi.org/10.1002/aic.15875

Ghanem, O.B., Shah, S.N., Leveque, J.M., Mutalib, M.I.A., El-Harbawi, M., Khan, A.S., Alnarabiji, M.S., Al-Absi, H.R.H., Ullah, Z., 2018. Study of the antimicrobial activity of cyclic cation-based ionic liquids via experimental and group contribution QSAR model. Chemosphere 195, 21-28. http://doi.org/10.1016/j.chemosphere.2017.12.018

Han, K., Ahn, C.K., Lee, M.S., Rhee, C.H., Kim, J.Y., Chun, H.D., 2013. Current

status and challenges of the ammonia-based CO_2 capture technologies toward commercialization. Int. J. Greenh. Gas Con. 14, 270-281. http://doi.org/10.1016/j.ijggc.2013.01.007

Higgins, S.J., Liu, Y.A., 2015. CO_2 capture modeling, energy savings, and heat pump integration. Ind. Eng. Chem. Res. 54, 2526-2553. http://doi.org/10.1021/ie504617w

Hu, X.T., Wang, J.W., Mei, M.C., Song, Z., Cheng, H.Y., Chen, L.F., Qi, Z.W., 2021. Transformation of CO_2 incorporated in adducts of N-heterocyclic carbene into dialkyl carbonates under ambient conditions: An experimental and mechanistic study. Chem. Eng. J. 413, 127469. http://doi.org/10.1016/j.cej.2020.127469

Huang, Y., Zhang, X.P., Zhang, X., Dong, H.F., Zhang, S.J., 2014. Thermodynamic modeling and assessment of ionic liquid-based CO_2 capture processes. Ind. Eng. Chem. Res. 53, 11805-11817. http://doi.org/10.1021/ie501538e

Iqbal, J., Muhammad, N., Rahim, A., Khan, A.S., Ullah, Z., Gonfa, G., Ahmad, P., 2019. COSMO-RS predictions, hydrogen bond basicity values and experimental evaluation of amino acid-based ionic liquids for lignocellulosic biomass dissolution. J. Mol. Liq. 273, 215-221. http://doi.org/10.1016/j.molliq.2018.10.044

Ješić, D., Lašič Jurković, D., Pohar, A., Suhadolnik, L., Likozar, B., 2021. Engineering photocatalytic and photoelectrocatalytic CO_2 reduction reactions: Mechanisms, intrinsic kinetics, mass transfer resistances, reactors and multi-scale modelling simulations. Chem. Eng. J. 407, 126799. http://doi.org/10.1016/j.cej.2020.126799

Jiang, C.H., Cheng, H.Y., Qin, Z.X., Wang, R.Z., Chen, L.F., Yang, C., Qi, Z.W., Liu, X.C., 2021. COSMO-RS prediction and experimental verification of 1,5-pentanediamine extraction from aqueous solution by ionic liquids. Green Energy Environ. 6, 422-431. http://doi.org/10.1016/j.gee.2020.12.011

Khan, A.S., Man, Z., Bustam, M.A., Gonfa, G., Chong, F.K., Ullah, Z., Nasrullah, A., Sarwono, A., Ahmad, P., Muhammad, N., 2017. Effect of structural variations on the thermophysical properties of protic ionic liquids: Insights from experimental and computational studies. J. Chem. Eng. Data 62, 2993-3003. http://doi.org/10.1021/acs.jced.6b00450

Khan, A.S., Sakina, Nasrullah, A., Ullah, S., Ullah, Z., Khan, Z., Khan, N.A., Khan, S.Z., Din, I.U., 2023. An overview on phytotoxic perspective of ionic liquids and deep eutectic solvents: The role of chemical structure in the phytotoxicity. ChemBioEng Rev. 10, 174-194. http://doi.org/10.1002/cben.202200033

Klamt, A., Eckert, F., 2000. COSMO-RS: A novel and efficient method for the a priori prediction of thermophysical data of liquids. Fluid Phase Equilib. 172, 43-72. http://doi.org/10.1016/S0378-3812(00)00357-5

Klamt, A., Jonas, V., Bürger, T., Lohrenz, J.C.W., 1998. Refinement and parametrization of COSMO-RS. J. Phys. Chem. A 102, 5074-5085. http://doi.org/10.1021/jp980017s

Kovačič, Ž., Likozar, B., Huš, M., 2020. Photocatalytic CO_2 reduction: A review of Ab initio mechanism, kinetics, and multiscale modeling simulations. ACS Catal. 10, 14984-15007. http://doi.org/10.1021/acscatal.0c02557

Li, G., Gui, C., Zhu, R., Lei, Z., 2021. Deep eutectic solvents for efficient capture of cyclohexane in volatile organic compounds: Thermodynamic and molecular mechanism. AIChE J. 68. http://doi.org/10.1002/aic.17535

Li, J., Chen, L.F., Ye, Y.M., Qi, Z.W., 2014. Solubility of CO_2 in the Mixed Solvent System of Alkanolamines and Poly(ethylene glycol) 200. J. Chem. Eng. Data 59, 1781-1787. http://doi.org/10.1021/je400947t

Linke, S., McBride, K., Sundmacher, K., 2020. Systematic green solvent selection for the hydroformylation of long-chain alkenes. ACS Sustainable Chem. Eng. 8, 10795-10811. http://doi.org/10.1021/acssuschemeng.0c02611

Liu, J.-L., Wang, X., Li, X.-S., Likozar, B., Zhu, A.-M., 2020a. CO_2 conversion, utilisation and valorisation in gliding arc plasma reactors. J. Phys. D: Appl. Phys. 53. http://doi.org/10.1088/1361-6463/ab7c04

Liu, Y., Yu, H., Sun, Y., Zeng, S., Zhang, X., Nie, Y., Zhang, S., Ji, X., 2020b. Screening deep eutectic solvents for CO_2 capture with COSMO-RS. Front. Chem. 8, 82. http://doi.org/10.3389/fchem.2020.00082

Liu, Y.R., Dai, Z.X., Zhang, Z.B., Zeng, S.J., Li, F.F., Zhang, X.P., Nie, Y., Zhang, L., Zhang, S.J., Ji, X.Y., 2021. Ionic liquids/deep eutectic solvents for CO_2 capture: Reviewing and evaluating. Green Energy Environ. 6, 314-328. http://doi.org/10.1016/j.gee.2020.11.024

Lu, T., Chen, F., 2012. Multiwfn: a multifunctional wavefunction analyzer. J. Comput. Chem. 33, 580-592. http://doi.org/10.1002/jcc.22885

Luo, F., Liu, X.L., Chen, S., Song, Y.F., Yi, X.Y., Xue, C.Y., Sun, L.Y., Li, J., 2021. Comprehensive evaluation of a deep eutectic solvent based CO_2 capture process through experiment and simulation. ACS Sustainable Chem. Eng. 9, 10250-10265. http://doi.org/10.1021/acssuschemeng.1c02722

Ma, T., Wang, J., Du, Z., Abdeltawab, A.A., Al-Enizi, A.M., Chen, X., Yu, G., 2017. A process simulation study of CO_2 capture by ionic liquids. Int. J. Greenh. Gas Con. 58, 223-231. http://doi.org/10.1016/j.ijggc.2017.01.017

Oexmann, J., Kather, A., 2010. Minimising the regeneration heat duty of post-combustion CO_2 capture by wet chemical absorption: The misguided focus on low heat of absorption solvents. Int. J. Greenh. Gas Con. 4, 36-43. http://doi.org/10.1016/j.ijggc.2009.09.010

Olugbemide, A.D., Oberlintner, A., Novak, U., Likozar, B., 2021. Lignocellulosic corn stover biomass pre-treatment by deep eutectic solvents (DES) for biomethane production process by bioresource anaerobic digestion. Sustainability. 13. http://doi.org/10.3390/su131910504

Paiva, A., Craveiro, R., Aroso, I., Martins, M., Reis, R.L., Duarte, A.R.C., 2014. Natural deep eutectic solvents - Solvents for the 21st century. ACS Sustainable Chem.

Eng. 2, 1063-1071. http://doi.org/10.1021/sc500096j

Pavlišič, A., Huš, M., Prašnikar, A., Likozar, B., 2020. Multiscale modelling of CO_2 reduction to methanol over industrial $Cu/ZnO/Al_2O_3$ heterogeneous catalyst: Linking ab initio surface reaction kinetics with reactor fluid dynamics. J. Clean Prod. 275. http://doi.org/10.1016/j.jclepro.2020.122958

Pinto, A.M., Rodriguez, H., Arce, A., Soto, A., 2014. Combined physical and chemical absorption of carbon dioxide in a mixture of ionic liquids. J. Chem. Thermodyn. 77, 197-205. http://doi.org/10.1016/j.jct.2013.10.023

Psarras, P.C., Comello, S., Bains, P., Charoensawadpong, P., Reichelstein, S., Wilcox, J., 2017. Carbon capture and utilization in the industrial sector. Environ. Sci. Technol. 51, 11440-11449. http://doi.org/10.1021/acs.est.7b01723

Qin, H., Song, Z., Cheng, H.Y., Deng, L.Y., Qi, Z.W., 2021. Physical absorption of carbon dioxide in imidazole-PTSA based deep eutectic solvents. J. Mol. Liq. 326. http://doi.org/10.1016/j.molliq.2021.115292

Qin, H., Wang, Z.H., Song, Z., Zhang, X., Zhou, T., 2022. High-throughput computational screening of ionic liquids for butadiene and butene separation. Processes. 10. http://doi.org/10.3390/pr10010165

Revelli, A.L., Mutelet, F., Jaubert, J.N., 2010. High carbon dioxide solubilities in imidazolium-based ionic liquids and in poly(ethylene glycol) dimethyl ether. J. Phys. Chem. B 114, 12908-12913. http://doi.org/10.1021/jp1057989

Sarmad, S., Mikkola, J.P., Ji, X., 2017. Carbon dioxide capture with ionic liquids and deep eutectic solvents: A new generation of sorbents. ChemSusChem. 10, 324-352. http://doi.org/10.1002/cssc.201600987

Silva, L.P., Fernandez, L., Conceicao, J.H.F., Martins, M.A.R., Sosa, A., Ortega, J., Pinho, S.P., Coutinho, J.A.P., 2018. Design and characterization of sugar-based deep eutectic solvents using conductor-like screening model for real solvents. ACS Sustainable Chem. Eng. 6, 10724-10734. http://doi.org/10.1021/acssuschemeng.8b02042

Singto, S., Supap, T., Idem, R., Tontiwachwuthikul, P., Tantayanon, S., Al-Marri, M.J., Benamor, A., 2016. Synthesis of new amines for enhanced carbon dioxide (CO_2) capture performance: The effect of chemical structure on equilibrium solubility, cyclic capacity, kinetics of absorption and regeneration, and heats of absorption and regeneration. Sep. Purif. Technol. 167, 97-107. http://doi.org/10.1016/j.seppur.2016.05.002

Song, Y.F., Chen, S., Luo, F., Sun, L.Y., 2020a. Absorption of toluene using deep eutectic solvents: quantum chemical calculations and experimental investigation. Ind. Eng. Chem. Res. 59, 22605-22618. http://doi.org/10.1021/acs.iecr.0c04986

Song, Z., Hu, X.T., Wu, H.Y., Mei, M.C., Linke, S., Zhou, T., Qi, Z.W., Sundmacher, K., 2020b. Systematic screening of deep eutectic solvents as sustainable separation media exemplified by the CO_2 capture process. ACS Sustainable Chem. Eng. 8, 8741-8751. http://doi.org/10.1021/acssuschemeng.0c02490

Song, Z., Hu, X.T., Zhou, Y.G., Zhou, T., Qi, Z.W., Sundmacher, K., 2019a. Rational design of double salt ionic liquids as extraction solvents: Separation of thiophene/n-octane as example. AIChE J. 65, e16625. http://doi.org/10.1002/aic.16625

Song, Z., Wang, J.W., Sundmacher, K., 2021. Evaluation of COSMO-RS for solid-liquid equilibria prediction of binary eutectic solvent systems. Green Energy Environ. 6, 371-379. http://doi.org/10.1016/j.gee.2020.11.020

Song, Z., Zhou, T., Qi, Z., Sundmacher, K., 2019b. Extending the UNIFAC model for ionic liquid–solute systems by combining experimental and computational databases. AIChE J. 66, e16821. http://doi.org/10.1002/aic.16821

Sun, J., Zhao, M., Huang, L., Zhang, T., Wang, Q., 2023. Recent progress on direct air capture of carbon dioxide. Curr. Opin. Green Sust. 40, 100752. http://doi.org/https://doi.org/10.1016/j.cogsc.2023.100752

Taheri, M., Dai, C.N., Lei, Z.G., 2018. CO_2 capture by methanol, ionic liquid, and their binary mixtures: Experiments, modeling, and process simulation. AIChE J. 64, 2168-2180. http://doi.org/10.1002/aic.16070

Taheri, M., Zhu, R.S., Yu, G.Q., Lei, Z.G., 2021. Ionic liquid screening for CO_2 capture and H2S removal from gases: The syngas purification case. Chem. Eng. Sci. 230, 116199. http://doi.org/10.1016/j.ces.2020.116199

Ullah, Z., Bustam, M.A., Man, Z., Khan, A.S., Muhammad, N., Sarwono, A., 2017. Preparation and kinetics study of biodiesel production from waste cooking oil using new functionalized ionic liquids as catalysts. Renew. Energ. 114, 755-765. http://doi.org/10.1016/j.renene.2017.07.085

Valderrama, J.O., Robles, P.A., 2007. Critical properties, normal boiling temperatures, and acentric factors of fifty ionic liquids. Ind. Eng. Chem. Res. 46, 1338-1344. http://doi.org/10.1021/ie0603058

Valderrama, J.O., Sanga, W.W., Lazzus, J.A., 2008. Critical properties, normal boiling temperature, and acentric factor of another 200 ionic liquids. Ind. Eng. Chem. Res. 47, 1318-1330. http://doi.org/10.1021/ie071055d

Wang, J.W., Cheng, H.Y., Song, Z., Chen, L.F., Deng, L.Y., Qi, Z.W., 2019. Carbon dioxide solubility in phosphonium-based deep eutectic solvents: An experimental and molecular dynamics study. Ind. Eng. Chem. Res. 58, 17514-17523. http://doi.org/10.1021/acs.iecr.9b03740

Wang, J.W., Song, Z., Cheng, H.Y., Chen, L.F., Deng, L.Y., Qi, Z.W., 2018. Computer-aided design of ionic liquids as absorbent for gas separation exemplified by CO_2 capture cases. ACS Sustainable Chem. Eng. 6, 12025-12035. http://doi.org/10.1021/acssuschemeng.8b02321

Wang, J.W., Song, Z., Cheng, H.Y., Chen, L.F., Deng, L.Y., Qi, Z.W., 2020a. Multilevel screening of ionic liquid absorbents for simultaneous removal of CO_2 and H2S from natural gas. Sep. Purif. Technol. 248. http://doi.org/10.1016/j.seppur.2020.117053

Wang, Z., Song, Z., Zhou, T., 2020b. Machine learning for ionic liquid toxicity prediction. Processes. 9. http://doi.org/10.3390/pr9010065

Xie, Y.J., Zhang, Y.Y., Lu, X.H., Ji, X.Y., 2014. Energy consumption analysis for CO2 separation using imidazolium-based ionic liquids. Appl. Energy 136, 325-335. http://doi.org/10.1016/j.apenergy.2014.09.046

Yan, Y.Z., Chen, C.C., 2010. Thermodynamic modeling of CO_2 solubility in aqueous solutions of NaCl and Na_2SO_4. J. Supercrit. Fluids 55, 623-634. http://doi.org/10.1016/j.supflu.2010.09.039

Yu, G., Mu, M., Li, J., Wu, B., Xu, R., Liu, N., Chen, B., Dai, C., 2020. Imidazolium-based ionic liquids introduced into π-electron donors: Highly efficient toluene capture. ACS Sustainable Chem. Eng. 8, 9058-9069. http://doi.org/10.1021/acssuschemeng.0c02273

Yu, G.Q., Dai, C.N., Wu, B., Liu, N., Chen, B.H., Xu, R.N., 2021. Chlorine drying with hygroscopic ionic liquids. Green Energy Environ. 6, 350-362. http://doi.org/10.1016/j.gee.2020.10.022

Zhang, W.X., Liu, X.B., Zhang, H.R., Li, S.H., Yang, J.W., Cui, P.Z., Zhu, Z.Y., Ma, Y.X., Wang, Y.L., 2019. Molecular dynamics evaluation of removal of acid gases from SNG by ionic liquid. ACS Sustainable Chem. Eng. 7, 18093-18104. http://doi.org/10.1021/acssuschemeng.9b05132

Zhang, Y.Y., Ji, X.Y., Lu, X.H., 2018. Choline-based deep eutectic solvents for CO_2 separation: Review and thermodynamic analysis. Renew. Sust. Energ. Rev. 97, 436-455. http://doi.org/10.1016/j.rser.2018.08.007

Zhang, Y.Y., Ji, X.Y., Xie, Y.J., Lu, X.H., 2016. Screening of conventional ionic liquids for carbon dioxide capture and separation. Appl. Energy 162, 1160-1170. http://doi.org/10.1016/j.apenergy.2015.03.071

Zhao, F., Cui, C.X., Dong, S.L., Xu, X.Y., Liu, H.L., 2023. An overview on the corrosion mechanisms and inhibition techniques for amine-based post-combustion carbon capture process. Sep. Purif. Technol. 304, 122091. http://doi.org/10.1016/j.seppur.2022.122091

Zhou, T., McBride, K., Linke, S., Song, Z., Sundmacher, K., 2020. Computer-aided solvent selection and design for efficient chemical processes. Curr. Opin. Chem. Eng. 27, 35-44. http://doi.org/10.1016/j.coche.2019.10.007